Doped Semiconductors

International Edition: DOI: 10.1002/anie.201702673
German Edition: DOI: 10.1002/ange.201702673

Size Dependence of Doping by a Vacancy Formation Reaction in Copper Sulfide Nanocrystals

Orian Elimelech, Jing Liu, Anna M. Plonka, Anatoly I. Frenkel, and Uri Banin**

Dedicated to Professor Dieter Fenske on the occasion of his 75th birthday

Abstract: *Doping of nanocrystals (NCs) is a key, yet underexplored, approach for tuning of the electronic properties of semiconductors. An important route for doping of NCs is by vacancy formation. The size and concentration dependence of doping was studied in copper(I) sulfide (Cu_2S) NCs through a redox reaction with iodine molecules (I_2), which formed vacancies accompanied by a localized surface plasmon response. X-ray spectroscopy and diffraction reveal transformation from Cu_2S to Cu-depleted phases, along with CuI formation. Greater reaction efficiency was observed for larger NCs. This behavior is attributed to interplay of the vacancy formation energy, which decreases for smaller sized NCs, and the growth of CuI on the NC surface, which is favored on well-defined facets of larger NCs. This doping process allows tuning of the plasmonic properties of a semiconductor across a wide range of plasmonic frequencies by varying the size of NCs and the concentration of iodine. Controlled vacancy doping of NCs may be used to tune and tailor semiconductors for use in optoelectronic applications.*

Optoelectronic properties of semiconductor nanocrystals (SC NCs) depend strongly on their size, composition, and shape.[1,2] High-level synthetic control of NCs, accompanied by their wet-chemical processability, has already led to their application as chromophores in displays, biological tagging, solar cells, sensors, and functional devices.[3–6] An important route to achieve additional control of optoelectronic properties is through doping by the introduction of donor or acceptor impurities,[7–9] which is the primary method used to control bulk semiconductor properties. Aliovalent impurity doping in NCs is challenging because of the difficulty associated with controlled introduction of foreign atoms into the SC NC lattice.[10] An alternative interesting route for doping is by vacancy formation. This approach is of particular importance when the insertion of impurities is difficult and especially instrumental in NCs made of materials with a tendency to form lattice vacancies, such as copper chalcogenides and metal oxides.[11–15]

Vacancy formation in these systems leads to the appearance of a localized surface plasmon resonance (LSPR) related to the free carriers, and is perhaps the most notable signature of vacancies.[16–18] The appearance of plasmonic behavior within such SC NCs opens a path for investigation of coupled plasmonic–excitonic behavior in quantum confined systems. The ability to control plasmonic properties with reversible redox reactions and vacancy control in metal-oxide NCs also provides a basis for implementing such materials in smart window technology.[6]

To date, most studies have reported the relation of plasmonic behavior in SC NCs to composition, defect content, and particle morphology and shape.[19] The size effect of the plasmonic response in these systems is convoluted together with the effect of the carrier concentration. In spherical metal NCs only the former can be utilized to control the plasmon in a given material system,[20,21] while for SC NCs both parameters are important.[22] Hence, there is a need to develop methods for controlling the plasmonic response by either NC size or carrier concentration and to separately understand their effects. To address these important questions we utilized quasi-spherical copper(I) sulfide (Cu_2S) NCs as a model system. Cu_2S and other copper chalcogenide NCs have been widely studied in recent years owing to their reduced toxicity, environmental compatibility, and their relevant band gap for photovoltaic applications (1.21 eV for bulk Cu_2S).[23–29] Doping by copper vacancy formation occurs readily because of the low chemical potential and high mobility of copper ions.[30] This transforms the stoichiometric Cu_2S phase to Cu-depleted $Cu_{2-x}S$ phases, also possibly undergoing structural transformation.[31] The vacancies in the doped NCs play the role of free holes and manifest p-type doped material properties with an LSPR feature appearing in the near-infrared (NIR). This doping process was performed using oxidation under air exposure[11] and also by strong oxidizers such as iodine molecules (I_2) for Cu_2S nanorods.[15] A process of thermal doping by copper vacancy formation in an array of 14 nm Cu_2S NCs was also recently reported by us.[32] Unlike common interfacial or surface defects, such vacancies are not trap sites and provide free carriers.

Herein, we study vacancy doping and the related plasmonic response in a Cu_2S NCs model system, focusing on NC size and vacancy concentration effects. We implement a post-synthetic chemical method involving copper(I) sulfide oxidation by I_2, which creates a copper(I) iodide (CuI) phase, thus

[*] O. Elimelech, Prof. U. Banin
The Institute of Chemistry and The Center for Nanoscience and Nanotechnology, The Hebrew University of Jerusalem
Jerusalem 91904 (Israel)
E-mail: Uri.Banin@mail.huji.ac.il
Dr. J. Liu, Dr. A. M. Plonka, Prof. A. I. Frenkel
Department of Materials Science and Chemical Engineering
Stony Brook University
Stony Brook, NY 11794 (USA)
E-mail: Anatoly.Frenkel@stonybrook.edu
Supporting information and the ORCID identification number(s) for the author(s) of this article can be found under: https://doi.org/10.1002/anie.201702673.

forming copper vacancies in a controlled manner and resulting in $Cu_{2-x}S$ NCs. Using a combination of optical absorption measurements, advanced structural characterization by synchrotron X-ray absorption and scattering methods, we studied the reaction mechanism, the plasmonic response, and the size and concentration dependence. We determined that the vacancy formation reaction efficiency increases with NC size; this is ascribed to an interplay between a thermodynamic size effect that energetically favors the formation of vacancies in smaller NCs, and a surface effect that stabilizes CuI islands more easily on the larger facets of larger NCs. With this chemical doping method, we can thus control the vacancy concentration and plasmonic response in Cu_2S NCs of different sizes and it is possible to reach a similar plasmon frequency by varying either parameter. However, larger NCs offer a wider range of spectral tunability for the LSPR response since they can support a higher vacancy concentration in a stable manner.

To study the effect of the NC size on the doping process and the LSPR response, a size-controlled synthesis for Cu_2S NCs was developed by modifying known procedures.[33–35] By controlling the growth time and the precursor concentration, a size series of highly monodisperse Cu_2S NCs was synthesized, with average diameters of 3, 7, 10, and 14 nm, as measured by transmission electron microscopy (TEM; Figure 1; see the Supporting Information for synthetic details).

The powder X-ray diffraction (XRD) pattern of the as-synthesized Cu_2S NCs fits the monoclinic low-chalcocite Cu_2S phase and no features corresponding to an LSPR were observed in the absorption spectrum. Upon air exposure, the NCs were oxidized and a transformation from pristine Cu_2S to Cu-depleted phases was detected by XRD. A significant LSPR feature appeared in the NIR because of copper vacancy formation and the related free holes (Supporting Information, Figure S1).

To investigate the optical and structural changes upon vacancy formation we used a chemical method for doping Cu_2S NCs that involved reaction with I_2.[15] The described reaction mechanism is a redox process in which I_2 oxidizes Cu_2S by leaching out Cu^+ ions to form CuI salt. The oxidized NCs are p-type doped because of the formation of copper vacancies while the sulfur anion backbone remains intact, leading to a Cu-depleted $Cu_{2-x}S$ phase [Eq. (1)]:

$$Cu_2S + 0.5\,n\,I_2 \rightarrow Cu_{2-n}S + n\,CuI \quad (1)$$

For the doping reaction the Cu_2S NCs were dispersed in chloroform and mixed with I_2 at different ratios of iodine to copper (I/Cu; see the Supporting Information for details on determination of the concentration ratio). Figure 1e shows the spectral behavior for 7 nm Cu_2S NCs. With increased I/Cu ratios the plasmonic peak intensity increased significantly and blue-shifted in response to an increased concentration of free holes. Within a time resolution of a few seconds, the changes in the spectra took place immediately following addition of I_2 and then remained stable.

To investigate the effect on the electrical properties, the I_2 treatment was also applied to an array of 7 nm Cu_2S NCs on a substrate by drop casting. Figure 1f presents I–V measurements before and after the reaction, manifesting an increase in the conductivity by about 7 orders of magnitude following treatment with I_2. This change is also well-correlated to the presence of free holes arising from copper vacancy formation.

The structural changes in the NCs were studied by synchrotron XRD measurements using 0.29 Å radiation. Cu_2S NCs (14 nm) were measured after I_2 treatment for different I/Cu ratios (Figure 2a; Supporting Information, Figure S3 for 7 nm NCs). The pure NCs exhibited an XRD pattern that matches the stoichiometric low-chalcocite Cu_2S phase. The XRD patterns of the I_2-treated NCs match the djurleite $Cu_{1.94}S$ phase for the lowest I/Cu ratios of 5% and 10%, and to the digenite $Cu_{1.80}S$ phase for a 30% I/Cu ratio. These transformations are well-visualized by a shift to higher angles for the main diffraction peaks of Cu_2S (Figure 2b). These results show that reaction with iodine atoms causes copper atoms to leach from the NCs to form copper vacancies, leading to the Cu-depleted phases.

The formation of crystalline CuI, the by-product of the reaction, was also detected by XRD. The ratio between the CuI and $Cu_{2-x}S$ peaks increases with the I/Cu ratio (Supporting Information, Figure S4). This observation is also in agreement with the suggested mechanism for the reaction: CuI forms at the expense of the $Cu_{2-x}S$ phases as the $Cu_{2-x}S$ NCs are the sole source of copper. When the solution contains more iodine than copper (150% I/Cu), the CuI phase dominates the XRD pattern, showing that for a very high I/Cu ratio the crystalline structure of the NCs is significantly compromised.

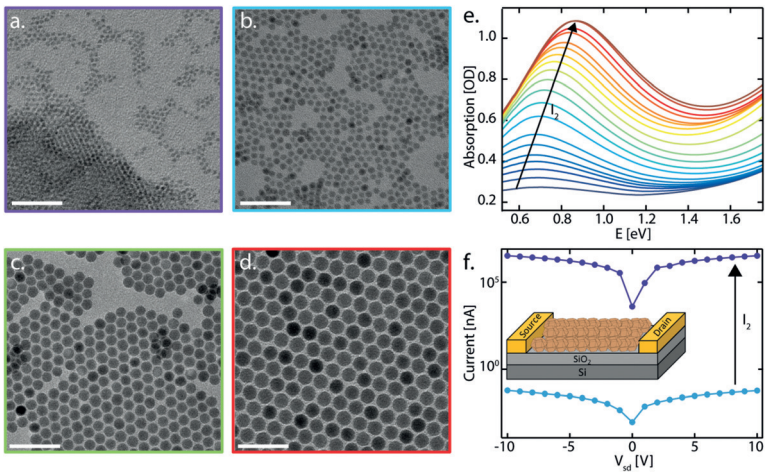

Figure 1. TEM images of as-synthesized Cu_2S NCs. Average diameters of the NCs: a) 3 nm, b) 7 nm, c) 10 nm, and d) 14 nm. Scale bars: 50 nm. e) Visible/near-infrared (VIS/NIR) absorption spectra of 7 nm Cu_2S NCs upon I_2 treatment. Increasing the I_2 concentration drives the formation of copper vacancies and development of the LSPR peak. The plasmon peak increases in intensity and is blue-shifted because of the increase in the free-charge carrier density. f) I–V measurement for the 7 nm Cu_2S NCs array before (blue) and after (purple) I_2 treatment of the array. The conductivity increases by about 7 orders of magnitude following the treatment because of the increase in the density of free holes.

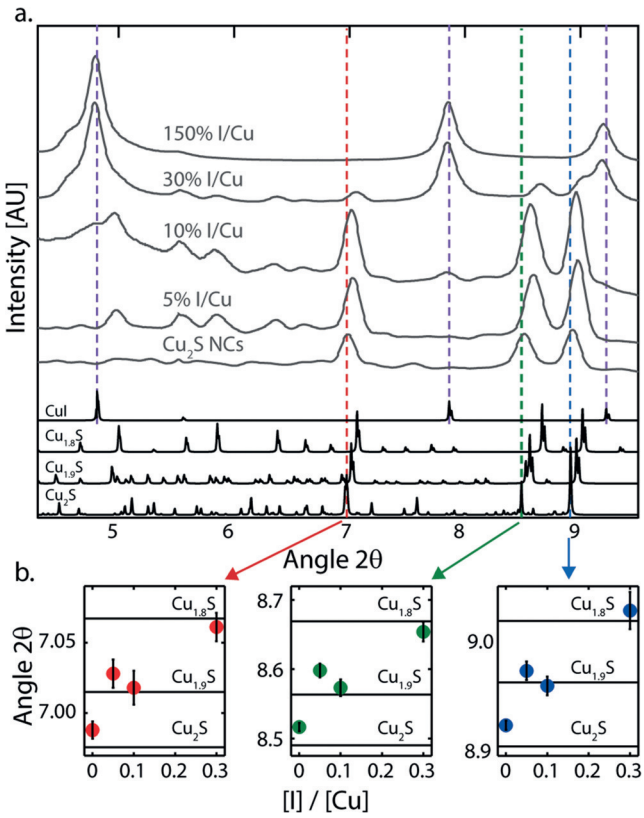

Figure 2. a) XRD data for 14 nm Cu_2S NCs following I_2 treatment at different I/Cu ratios. The relevant reference spectra are shown below. The initial phase of NCs is low-chalcocite Cu_2S. The reaction with I_2 forms a crystalline CuI phase (angles marked with a dashed purple line) at the expense of the Cu_2S phase. b) Dependence of the angles of three main diffraction Cu_2S peaks on the I/Cu ratio in the reaction ((102) (●), (110) (●), (103) (●), in Cu_2S). Increasing the I/Cu ratio forms copper vacancies, leading to transformation of the NCs to Cu-depleted phases. Reference values for angles of the main diffraction peaks appear as horizontal lines.

In addition to the XRD measurements, X-ray absorption fine structure (XAFS) spectroscopy measurements, including X-ray absorption near-edge structure (XANES) and extended XAFS (EXAFS), were conducted to investigate the changes in the local chemical environment of copper and iodine atoms. While XRD is predominantly sensitive to the crystalline phase, and the diffraction peaks become broader and less informative for small NCs, XAFS has excellent spatial and chemical sensitivities to the local environment irrespective of the degree of crystalline order. Figures 3a and b present copper K-edge XAFS spectra for 14 nm Cu_2S NCs following treatment with I_2 at different I/Cu ratios. The local environment of the copper atoms is composed of two phases—Cu_2S and CuI—as was observed from the XAFS signal (Figure 3a). The presence of isosbestic points supports the mechanism of formation of one phase at the expense of the other.

The contribution of Cu–S and Cu–I pairs to the copper K-edge EXAFS data are visualized in the R-space plot obtained by Fourier transform (Figure 3b). As the I/Cu ratio increases, the peak at 1.8 Å corresponding to Cu–S bonds decreases in intensity and the peak at 2.4 Å corresponding to Cu–I bonds increases. No evidence was found for Cu–Cu metallic bonding.

Iodine K-edge XAFS measurements complement the copper K-edge results from the iodine point of view. The local environment of iodine atoms in the treated NCs is the same as that in bulk CuI powder, as was observed from the XAFS measurements (Supporting Information, Figure S5b). Iodine has one type of nearest neighbor, copper, contributing to the peak at 2.2 Å in the R-space plot (Figure 3c). Furthermore, the peak amplitude in R-space increases with an increasing I/Cu ratio because of the monotonic dependence of the EXAFS function $\chi(R)$ on the coordination number.[36,37] For a higher I/Cu ratio, the CuI region becomes larger, the surface-to-volume ratio decreases, and the average Cu–I coordination number increases towards its maximum value of 4 in bulk CuI (Figure 3d).

Similar measurements were also conducted for 7 nm Cu_2S NCs (Supporting Information, Figure S5). Summarizing the analysis for the 14 and the 7 nm doped NCs at the same range of I/Cu ratios, Figure 3d presents the changes in the relative I–Cu coordination number N_I (normalized by the bulk coordination number of 4) extracted from the nonlinear least squares fitting for the iodine K-edge data (see the Supporting Information for a detailed analysis). The CuI phase fraction was calculated by linear combination analysis for the copper K-edge XANES signal using pure Cu_2S NCs and CuI powder as standards (Supporting Information, Figure S7), and its dependence on the I/Cu ratio is summarized in Figure 3e. Generally, the CuI phase becomes more dominant when the I/Cu ratio increases.

Both parameters, N_I and CuI phase fractions, are size dependent. While the absolute value of N_I in the 7 nm NCs increased gradually from 2.3 to 3.3 with an increase in the I/Cu ratio, for the 14 nm NCs a high, weakly varying coordination number was observed. The copper atom perspective showed a complementary behavior: in the 14 nm NCs, the CuI fraction continuously increased at the expense of the Cu_2S phase, manifesting a gradual change in the copper local environment, while the smaller 7 nm NCs showed only a minor change and reached a saturation value early on.

These observations can be explained by growth of the CuI nanocrystalline phase on the NC surface. On the surface of larger NCs, larger crystals of CuI can grow. The growth of larger CuI crystals requires the migration of more copper atoms from the NC to the new CuI phase. This is reflected by a significant change in the copper local environment, from the initial Cu_2S phase that contains only Cu–S bonds to the new phase that is rich in Cu–I bonds. However, since the CuI crystals are already large, the iodine coordination number is already close to that of the bulk at low relative I/Cu ratios, and the change in its coordination number value is negligible. For the same reason, only small CuI crystals grow on the 7 nm NCs surface. The growth of small CuI crystals requires a small amount of copper from the NCs, which keeps the copper local environment nearly the same as that in the NCs. The changes for iodine are more drastic since any addition of I_2 increases the volume-to-surface ratio of the small nanocrystalline phase of CuI and therefore significantly increases the coordination number.

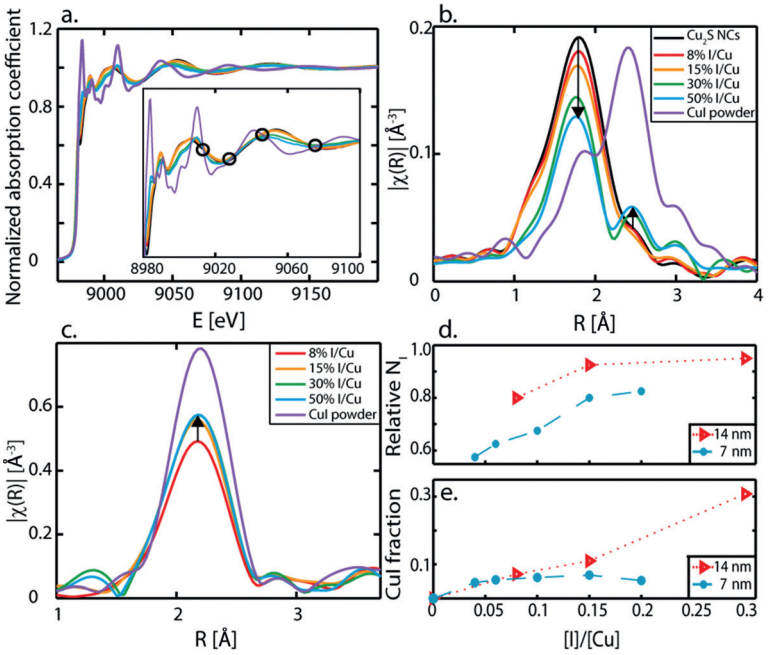

Figure 3. XAFS data for 14 nm Cu_2S NCs upon I_2 treatment. a) Copper K-edge XANES spectra and b) R-space plot for the copper K-edge EXAFS of 14 nm NCs shows a gradual development in the CuI phase at the expense of the Cu_2S phase. c) The R-space plots for the iodine K-edge EXAFS signal shows a minor change. d) Summary of data from XAFS analysis of 14 and 7 nm NCs. The relative amount of CuI from the I—Cu coordination number (N_I) perspective increases strongly with the I/Cu ratio of the 7 nm NCs (●), while the 14 nm NCs showed a high and weakly varying value (▲). e) From the copper atom perspective, for the 14 nm NCs the CuI phase fraction increases gradually with an increase of Cu/I ratio (▲) manifesting a notable change in the copper local environment, while the 7 nm NCs showed only a minor change and the value reached saturation early on (●).

Structural characterization clearly showed the formation of crystalline CuI following I_2 treatment of the Cu_2S NCs, and also the transformation to copper-depleted phases correlated to vacancy formation. The main change in the optical properties of the I_2-treated Cu_2S NCs is the development of the LSPR. The free-charge carrier density can be calculated from the Drude model [Eq. (2)]:[22]

$$N_h = \frac{\varepsilon_0 m_h(\varepsilon_\infty + 2\varepsilon_m)}{e^2\hbar^2}(E_{sp}^2 + \gamma^2) \qquad (2)$$

where N_h is the density of free holes, ε_0 is the vacuum dielectric constant, m_h is the hole mass in Cu_2S, ε_∞ is the high frequency dielectric constant of Cu_2S, ε_m is the dielectric constant of the medium (chloroform), e is the elementary charge, $\hbar$ is Planck's constant divided by 2π, E_{sp} is the plasmon energy, and γ is the damping parameter. The plasmon peaks were fitted using a Drude dielectric function model[22] (see the Supporting Information for details on the model and analysis, Section 7 and Figure S8) from which the plasmon energy (the peak maximum) and the damping parameter (effective peak width) were obtained. Subsequently, the density of free holes was calculated for each I/Cu ratio using Equation (2). This model and a Gaussian fit model provided similar results (Supporting Information, Figures S9 and S10). We note that the optical properties of the NCs are barely affected by the formation of CuI upon increasing the I/Cu ratio. This is because the $Cu_{2-x}S$–CuI band alignment is a type-I band offset and CuI has a large band gap (3 eV), which means that the electron–hole states are dictated mainly by the $Cu_{2-x}S$ phases. Moreover, the dielectric constant of CuI is similar to that of chloroform (4.5 and 4.8, respectively).[38–40]

As shown in Figure 4a for the Cu_2S NCs size series, the N_h value increases linearly with the I/Cu ratio. For larger NCs, larger I/Cu ratios were accessible because of their more robust structural stability (which is supported by the XRD data; Figure 2b; Supporting Information, Figure S3). Moreover, larger NCs were able to support higher hole concentrations. The slopes represent the doping reaction efficiency; that is, the number of holes per copper atom (holes/Cu) that were formed versus the I/Cu ratio that was introduced to the NCs solution. Figure 4b presents the doping reaction efficiency as a function of the NC diameter. The efficiency increases with NC size, from approximately 0.2 for the 3 nm NCs, to about 0.4 for the 14 nm NCs.

Small NCs are known for their higher reactivity; indeed, for metal NCs the energy of vacancy formation was reported to increase with size.[41,42] Yet the above analysis showed that the larger NCs react with I_2 and undergo the doping process more efficiently. Therefore the doping reaction also depends on an additional process that has an opposite relation to NC size. The vacancy formation is also related to the formation of crystalline CuI; without the latter the former could not exist. The growth of the CuI nanocrystalline phase is facilitated by both the larger NC surface area and the better defined facets on the NC surface—both of them increase with the NC size. Larger crystals grow on better defined facets as a consequence of a universal effect of elastic instability of curved surfaces that lowers the dimensionality of the crystals grown on such surfaces.[43] The growth of CuI on the surface of the NC is inferred from the EXAFS results (Figure 3d) and also directly evidenced from scanning transmission electron microscopy (STEM), showing a CuI nanocrystalline phase covering the NCs (Supporting Information, Figures S11 and S12).

The doping reaction efficiency is thus influenced by the interplay of both factors: the thermodynamic effect of the energy of vacancy formation and the surface effect. The observed trend (Figure 4b) demonstrates that the surface-area effect dominates the behavior of the reaction efficiency.

The LSPR of vacancy-doped NCs depends on the doping level and also on the NC size. The absorption data showed that the concentration of free holes increases with increasing I/Cu ratio. This is because the I/Cu ratio dictates the vacancy concentration. However, for the same I/Cu ratio the plasmon energy depends also on the NC size. This offers an additional dial with which to control the plasmon response in vacancy-doped SC NCs that is not available in the widely studied noble-metal nanoparticles.

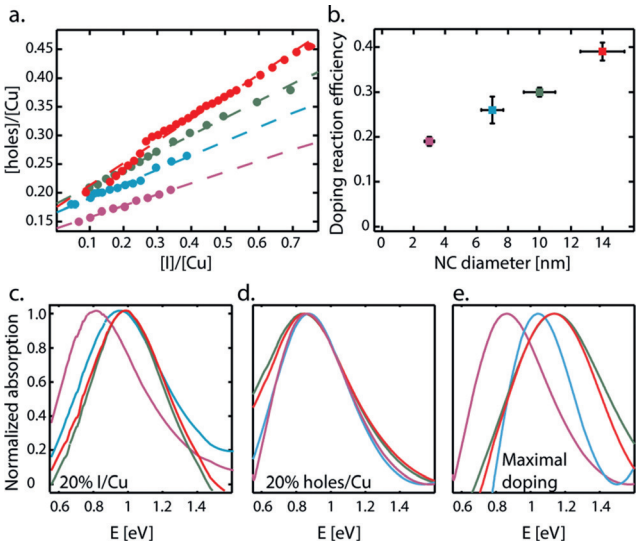

Figure 4. Size and concentration dependence of the doping reaction. a) The holes/Cu ratio increases linearly with the I/Cu ratio; the slope represents the doping reaction efficiency for each NC size. b) The doping reaction efficiency increases with NC diameter. c) Absorption spectra of I_2-treated NCs with a ratio of 20% I/Cu. Different sizes of NCs exhibit different energies of the LSPR from 0.82 eV (for 3 nm NCs) to 1 eV (for 14 nm NCs). Generally, the plasmon is red-shifted for the smaller NCs. d) Absorption spectra of the I_2-treated NCs with a 20% holes/Cu ratio. The plasmon energy is similar for different sizes (ca. 0.85 eV). e) Absorption spectra of maximally doped NCs. The maximal doping level of the NCs increases with size and the plasmon energy is blue-shifted from 0.85 to 1.15 eV. Key: 14 nm (——), 10 nm (——), 7 nm (——), 3 nm (——).

Figure 4c presents the LSPR response of the Cu_2S NCs size series that was treated with 20% I/Cu. While the LSPR features of the 10 and 14 nm NCs are nearly overlapping, a general trend of a red-shift in the plasmon peak with decreasing NC size is observed. This trend also correlates with a decrease in the doping level, reflecting the size dependence of the vacancy formation reaction efficiency. Therefore, for the same I/Cu ratio, the energy of the plasmon can be tuned by changing the NC size. A LSPR with a specific energy can be achieved for all sizes by varying the I/Cu ratio while the concentration of holes remains the same. Figure 4d presents the LSPR response of the Cu_2S NCs size series at a doping level of 20% holes/Cu where the I/Cu ratio is different for each size (ca. 10% for the large 14 nm NCs and up to 30% for the small 3 nm NCs). Above a specific size-dependent I/Cu ratio the intensity of the plasmon response decreases because of aggregation of the NCs. The maximal I/Cu ratio is different for each size and also the achieved doping level. Generally, larger NCs can support higher doping levels and exhibit LSPR at higher energy (Figure 4e).

In summary, we studied size effect on the vacancy doping process in Cu_2S NCs. The chemical efficiency of the reaction for vacancy formation was found to be size dependent with higher efficiency for the larger NCs. This results from interplay between the thermodynamic contribution, which decreases the energy of vacancy formation for smaller NCs, and a surface effect that favors the growth of a crystalline CuI phase on the defined surface facets of the larger NCs. Reaction with I_2 is thus a powerful and simple method for tuning the plasmonic properties of doped $Cu_{2-x}S$ NCs, even for strongly confined structures such as the 3 nm NCs. The plasmonic response can be tuned either by the size of NCs or by the doping level of holes, which is governed by the I/Cu ratio. This provides a wide range of tunable plasmonic frequencies in the NIR region for the same material. The ability to control vacancy doping in Cu_2S NCs, as demonstrated herein, points to similar possibilities in other copper chalcogenide and metal-oxide NCs of various shapes, sizes, and compositions, and also with other oxidizing agents. These findings open a path for precise control of vacancy concentrations in related NCs that may facilitate incorporation of such materials into optoelectronic applications.

Acknowledgements

The research leading to these results received funding through the NSF-BSF International Collaboration in Chemistry program. O.E., J.L., A.M.P., A.I.F., and U.B. acknowledge support of this work by NSF Grant No. CHE-1719534 and BSF Grant No. 2013/610. Use of the National Synchrotron Light Source II (beamline 28-ID-2) was supported by the U.S. Department of Energy (DOE) under Contract No. DE-SC0012704. XAFS experiments were performed at the DuPont-Northwestern-Dow Collaborative Access Team (DND-CAT) located at Sector 5 of the Advanced Photon Source (APS). DND-CAT is supported by Northwestern University, E.I. DuPont de Nemours & Co., and The Dow Chemical Company. XAFS measurements used resources of the APS, a DOE Office of Science User Facility operated for the DOE Office of Science by Argonne National Laboratory under Contract No. DE-AC02-06CH11357.

Conflict of interest

The authors declare no conflict of interest.

Keywords: copper sulfide nanocrystals · doping · surface plasmon resonance · vacancies

How to cite: *Angew. Chem. Int. Ed.* **2017**, *56*, 10335–10340
Angew. Chem. **2017**, *129*, 10471–10476

[1] M. V. Kovalenko, L. Manna, A. Cabot, Z. Hens, D. V. Talapin, C. R. Kagan, V. I. Klimov, A. L. Rogach, P. Reiss, D. J. Milliron, et al., *ACS Nano* **2015**, *9*, 1012–1057.
[2] A. Sitt, I. Hadar, U. Banin, *Nano Today* **2013**, *8*, 494–513.
[3] C. R. Kagan, E. Lifshitz, E. H. Sargent, D. V. Talapin, *Science* **2016**, *353*, aac5523-1-9.
[4] H. W. Hillhouse, M. C. Beard, *Curr. Opin. Colloid Interface Sci.* **2009**, *14*, 245–259.
[5] D. V. Talapin, C. B. Murray, *Science* **2005**, *310*, 86–89.
[6] A. Llordés, G. Garcia, J. Gazquez, D. J. Milliron, *Nature* **2013**, *500*, 323–327.
[7] D. J. Norris, A. L. Efros, S. C. Erwin, *Science* **2008**, *319*, 1776–1779.

[8] D. Mocatta, G. Cohen, J. Schattner, O. Millo, E. Rabani, U. Banin, *Science* **2011**, *332*, 77 – 81.
[9] A. Wolf, T. Kodanek, D. Dorfs, *Nanoscale* **2015**, *7*, 19519 – 19527.
[10] G. M. Dalpian, J. R. Chelikowsky, *Phys. Rev. Lett.* **2006**, *96*, 226802.
[11] J. M. Luther, P. K. Jain, T. Ewers, A. P. Alivisatos, *Nat. Mater.* **2011**, *10*, 361 – 366.
[12] C. Urso, M. Barawi, R. Gaspari, G. Sirigu, I. Kriegel, M. Zavelani-Rossi, F. Scotognella, M. Manca, M. Prato, L. De Trizio, et al., *J. Am. Chem. Soc.* **2017**, *139*, 1198 – 1206.
[13] N. B. Saleh, D. J. Milliron, N. Aich, L. E. Katz, H. M. Liljestrand, M. J. Kirisits, *Sci. Total Environ.* **2016**, *568*, 926 – 932.
[14] V. Lesnyak, R. Brescia, G. C. Messina, L. Manna, *J. Am. Chem. Soc.* **2015**, *137*, 9315 – 9323.
[15] P. K. Jain, K. Manthiram, J. H. Engel, S. L. White, J. A. Faucheaux, A. P. Alivisatos, *Angew. Chem. Int. Ed.* **2013**, *52*, 13671 – 13675; *Angew. Chem.* **2013**, *125*, 13916 – 13920.
[16] S. D. Lounis, E. L. Runnerstrom, A. Llordes, D. J. Milliron, *J. Phys. Chem. Lett.* **2014**, *5*, 1564 – 1574.
[17] A. Comin, L. Manna, *Chem. Soc. Rev.* **2014**, *43*, 3957 – 3975.
[18] R. J. Mendelsberg, G. Garcia, H. Li, L. Manna, D. J. Milliron, *J. Phys. Chem. C* **2012**, *116*, 12226 – 12231.
[19] A. Agrawal, I. Kriegel, D. J. Milliron, *J. Phys. Chem. C* **2015**, *119*, 6227 – 6238.
[20] P. K. Jain, M. A. El-Sayed, *Chem. Phys. Lett.* **2010**, *487*, 153 – 164.
[21] T. K. Sau, A. L. Rogach, F. Jäckel, T. A. Klar, J. Feldmann, *Adv. Mater.* **2010**, *22*, 1805 – 1825.
[22] J. A. Faucheaux, A. L. D. Stanton, P. K. Jain, *J. Phys. Chem. Lett.* **2014**, *5*, 976 – 985.
[23] Y. Wu, C. Wadia, W. Ma, B. Sadtler, A. P. Alivisatos, *Nano Lett.* **2008**, *8*, 2551 – 2555.
[24] G. Liu, T. Schulmeyer, J. Brotz, A. Klein, W. Jaegermann, *Thin Solid Films* **2003**, *431 – 432*, 477 – 482.
[25] K. Vinokurov, O. Elimelech, O. Millo, U. Banin, *ChemPhysChem* **2016**, *17*, 675 – 680.
[26] S. Wang, A. Riedinger, H. Li, C. Fu, H. Liu, L. Li, T. Liu, L. Tan, M. J. Barthel, G. Pugliese, et al., *ACS Nano* **2015**, *9*, 1788 – 1800.
[27] Y. Bekenstein, O. Elimelech, K. Vinokurov, O. Millo, U. Banin, *Z. Phys. Chem.* **2015**, *229*, 179 – 190.
[28] W. Van der Stam, A. C. Berends, C. De Mello Donega, *ChemPhysChem* **2016**, *17*, 559 – 581.
[29] Y. X. Zhao, C. Burda, *Energy Environ. Sci.* **2012**, *5*, 5564 – 5576.
[30] Y. Zhao, H. Pan, Y. Lou, X. Qiu, J. Zhu, C. Burda, *J. Am. Chem. Soc.* **2009**, *131*, 4253 – 4261.
[31] Y. Xie, A. Riedinger, M. Prato, A. Casu, A. Genovese, P. Guardia, S. Sottini, C. Sangregorio, K. Miszta, S. Ghosh, et al., *J. Am. Chem. Soc.* **2013**, *135*, 17630 – 17637.
[32] Y. Bekenstein, K. Vinokurov, S. Keren-Zur, I. Hadar, Y. Schilt, U. Raviv, O. Millo, U. Banin, *Nano Lett.* **2014**, *14*, 1349 – 1353.
[33] W. Han, L. Yi, N. Zhao, A. Tang, M. Gao, Z. Tang, *J. Am. Chem. Soc.* **2008**, *130*, 13152 – 13161.
[34] T. Kuzuya, S. Yamamuro, T. Hihara, K. Sumiyama, *Chem. Lett.* **2004**, *33*, 352 – 353.
[35] M. J. Turo, J. E. Macdonald, *ACS Nano* **2014**, *8*, 10205 – 10213.
[36] M. Newville, *Rev. Mineral. Geochem.* **2014**, *78*, 33 – 74.
[37] A. I. Frenkel, *Chem. Soc. Rev.* **2012**, *41*, 8163 – 8178.
[38] A. Klein, *J. Phys. Condens. Matter* **2015**, *27*, 134201.
[39] I. Konovalov, L. Makhova, *J. Appl. Phys.* **2008**, *103*, 103702.
[40] O. Madelung, *Semicond. Data Handbook*, Springer, Heidelberg, **2004**, p. 944.
[41] W. H. Qi, M. P. Wang, *J. Mater. Sci.* **2004**, *39*, 2529 – 2530.
[42] N. T. Gladkikh, A. P. Kryshtal, S. I. Bogatyrenko, *Tech. Phys.* **2010**, *55*, 1657 – 1660.
[43] G. Meng, J. Paulose, D. R. Nelson, V. N. Manoharan, *Science* **2014**, *343*, 634 – 637.

Manuscript received: March 14, 2017
Revised manuscript received: May 29, 2017
Accepted manuscript online: June 22, 2017
Version of record online: July 19, 2017

